

1 Effects of aquifer geometry on seawater intrusion in annulus
2 segment island aquifers

3
4 Zhaoyang Luo^{1,2}, Jun Kong^{1,3,#}, Chengji Shen¹, Pei Xin¹, Chunhui Lu¹, Ling Li⁴,
5 David Andrew Barry²

6
7 ¹State Key Laboratory of Hydrology-Water Resources and Hydraulic Engineering, Hohai
8 University, Nanjing, China

9
10 ²Ecological Engineering Laboratory (ECOL), Environmental Engineering Institute (IIE),
11 Faculty of Architecture, Civil and Environmental Engineering (ENAC), École Polytechnique
12 Fédérale de Lausanne (EPFL), Lausanne, Switzerland

13
14 ³Jiangsu Key Laboratory of Coast Ocean Resources Development and Environment Security,
15 Hohai University, Nanjing, China

16
17 ⁴School of Engineering, Westlake University, Hangzhou, China

18
19 #Corresponding author: Jun Kong (kongjun999@126.com)

20
21 Resubmitted to *Hydrology and Earth System Sciences* on ~~8 November~~ 2021

Deleted: 27

Deleted: 9

Deleted: August

25 **Abstract**

26 Seawater intrusion in island aquifers was considered analytically, specifically for annulus
27 segment aquifers (ASAs), i.e., aquifers that (in plan) have the shape of an annulus segment.
28 Based on the Ghijben-Herzberg and hillslope-storage Boussinesq equations, analytical
29 solutions were derived for steady-state seawater intrusion in ASAs, with a focus on the
30 freshwater-seawater interface and its corresponding watertable elevation. Predictions of the
31 analytical solutions compared well with experimental data, and so they were employed to
32 investigate the effects of aquifer geometry on seawater intrusion in island aquifers. Three
33 different ASA geometries were compared: convergent (smaller side facing the lagoon),
34 rectangular and divergent (larger side facing the sea). Depending on the aquifer geometry,
35 seawater intrusion was found to vary greatly, such that the assumption of a rectangular aquifer
36 to model an ASA can lead to poor estimates of seawater intrusion. Other factors being equal,
37 compared with rectangular aquifers, seawater intrusion is more extensive and watertable
38 elevation is lower in divergent aquifers, with the opposite tendency in convergent aquifers.
39 Sensitivity analysis further indicated that the effects of aquifer geometry on seawater intrusion
40 and watertable elevation vary with aquifer width and distance from the circle center to the
41 inner arc (the lagoon boundary for convergent aquifers while the internal no-flow boundary
42 for divergent aquifers). A larger aquifer width and distance from the circle center to the inner
43 arc weaken the effects of aquifer geometry and hence differences in predictions for the three
44 geometries become less pronounced.

45 **Keywords:** sharp-interface; steady-state analytical solution; atoll aquifer; annulus segment
46 aquifer, seawater intrusion

47 **Key Points**

- 48 ➤ Analytical solutions of steady-state seawater intrusion were derived for annulus segment
49 aquifers
- 50 ➤ Among three different aquifer geometries, divergent aquifers have the lowest watertable
51 and hence the most extensive seawater intrusion
- 52 ➤ Aquifer geometry effects on seawater intrusion depend on the aquifer width and distance
53 from the circle center to the inner arc

1. Introduction

Islands are extensively distributed throughout the world's oceans. Unfortunately, their groundwater resources are impacted by sea-level rise and increased demands. According to a recent estimate, there are approximately 65 million people living in oceanic islands where groundwater may be the only source of freshwater (Thomas et al., 2020). Fresh groundwater stored on oceanic islands is mainly from precipitation (usually in the form of a freshwater lens) and its availability varies due to different factors, e.g., island topography, rainfall patterns, tides, episodic storms and human activities (White & Falkland, 2010; Storlazzi et al., 2018). Seawater intrusion is thus an important issue due to its deleterious effect on oceanic island freshwater storage (e.g., Werner et al., 2017; Lu et al., 2019; Memari et al., 2020).

In contrast to coastal aquifers where seawater intrudes into freshwater from one direction only, seawater intrusion occurs from four directions for narrow strip islands and from all directions for circular islands. Over the past few decades, seawater intrusion in oceanic islands has been extensively investigated in field observations (e.g., Röper et al., 2013; Post et al., 2019), laboratory experiments (e.g., Stoeckl et al., 2015; Bedekar et al., 2019; Memari et al., 2020), numerical simulations (e.g., Lam, 1974; Gingerich et al., 2017; Liu & Tokunaga, 2019) and analytical solutions (e.g., Fetter, 1972; Ketabchi et al., 2014; Lu et al., 2019).

Among these, analytical solutions are effective tools to assess the extent of seawater intrusion (i.e., the location of the freshwater-seawater interface), although they cannot incorporate complex factors (e.g., dispersive mixing and transient oceanic dynamics) (Werner et al., 2013). The advantages of analytical solutions are that they are computationally efficient, can

Deleted: two

76 be used as test cases for numerical models, and can reveal the explicit relationships between
77 parameters that influence seawater intrusion (e.g., Fetter, 1972; Ketabchi et al., 2014; Liu et
78 al., 2014; Lu et al., 2019;).

79 Based on the Dupuit-Forchheimer approximation (i.e., ignoring vertical flow) and the
80 Ghijben-Herzberg equation (Drabbe & Badon Ghijben, 1889, English translation given by
81 Post (2018); Herzberg, 1901), Fetter (1972) presented analytical solutions describing the
82 freshwater-seawater interface location and watertable elevation in a circular island. Bailey et
83 al. (2010) further compared these single-layered analytical solutions with field measurements,
84 indicating that the analytical solutions perform well in estimating the freshwater-seawater
85 interface location and watertable elevation. Fetter's solutions formed the foundation for many
86 subsequent analytical studies on seawater intrusion in island aquifers. Again, for a single
87 layer, Chesnaux and Allen (2008) and Greskowiak et al. (2013) developed analytical solutions
88 to predict the steady-state groundwater age distribution in freshwater lenses. In addition, using
89 single-layered analytical solutions, Morgan and Werner (2014) proposed vulnerability
90 indicators of freshwater lenses under sea-level rise and recharge change.

91 Since aquifers are usually heterogeneous, the single-layer analytical solutions were
92 subsequently extended to two-layered island aquifers. Vacher (1988) derived solutions for the
93 freshwater-seawater interface location and watertable elevation for infinite-strip islands
94 composed of different layers. Dose et al. (2014) conducted laboratory experiments to validate
95 and confirm the reliability of analytical solutions proposed by Fetter (1972) and Vacher
96 (1988). Ketabchi et al. (2014) extended Fetter's analytical solutions to calculate the

97 freshwater-seawater interface location and watertable elevation in two-layered circular islands
98 subject to sea-level rise. Their results indicated that land-surface inundation caused by sea-
99 level rise has a considerable impact on fresh groundwater lenses. Recently, Lu et al. (2019)
100 derived analytical solutions for the freshwater-seawater interface location and watertable
101 elevation for both strip and circular islands with two adjacent layers, i.e., a less permeable
102 slice along the shoreline of an island, and a more permeable zone inland.

103 All the abovementioned analytical solutions apply to either strip or circular islands.
104 According to the classification of sand dunes developed by Stuyfzand (1993; 2017), there are
105 different island layouts that should be considered, e.g., where the shape of the island is an
106 annulus segment, instead of a strip or circular disk (Figure 1). Annulus segment-shaped
107 islands are found in various atolls (i.e., circular chains of islands surrounding a central
108 lagoon) as found in the Pacific and Indian Oceans (Werner et al., 2017; Duvat, 2019).
109 Nevertheless, analytical solutions of seawater intrusion are not yet available for annulus
110 segment aquifers (ASAs). In general, ASAs are conceptually treated as a 2D cross section,
111 similar to strip islands (e.g., Ayers & Vacher, 1986; Underwood et al., 1992; Bailey et al.,
112 2009; Werner et al., 2017). Evidently, topography plays an important role in groundwater flow
113 and hence seawater intrusion (e.g., Zhang et al., 2016; Liu & Tokunaga, 2019). It remains
114 unclear whether analytical solutions of seawater intrusion for strip islands are appropriate for
115 ASAs. It is moreover additionally unclear how island geometry affects the freshwater-
116 seawater interface location and watertable elevation of ASAs.

117 In this study, analytical solutions are derived for steady-state seawater intrusion for ASAs,

118 with a focus on the freshwater-seawater interface location and its corresponding watertable
119 elevation. After comparing their predictions with experimental data (Memari et al., 2020), the
120 analytical solutions are employed to investigate the effects of aquifer geometry on the
121 freshwater-seawater interface location and watertable elevation in ASAs.

122 2. Conceptual Model

123 Figure 2 shows the conceptual model of an ASA (a slice of an atoll island). The plan
124 view of the model domain is represented as a sector ($EFGH$) with an angle θ (Figure 2a).
125 Radial flow only is considered. The sea (EF) and lagoon (HG) boundaries are located at $L +$
126 L_0 [L] and L_0 [L] from the circle center, respectively. Since the longitudinal length is usually
127 much longer than the lateral length for an atoll island (Werner et al., 2017), seawater intrusion
128 from the lateral sides (EH and FG , Figure 2a) is negligible in comparison to the longitudinal
129 side, especially for the middle portion of an ASA. Therefore, EH and FG are treated as lateral
130 no-flow boundaries. Note that treating the lateral sides as no-flow boundaries is often used in
131 studies of freshwater lenses on atoll islands (e.g., Ayers & Vacher, 1986; Underwood et al.,
132 1992; Bailey et al., 2009; Werner et al., 2017). The side view of the model domain is
133 conceptualized as a rectangle ($ABCD$) along the radial direction with dimensions of L [L]
134 (width) $\times d$ [L] (height) (Figure 2b, c). AD is the impermeable base while BC is the land
135 surface through which aquifer recharge flows.

136 Both the sea and lagoon water levels are set to H_s [L], which results in an internal no-
137 flow boundary (water divide, where the slope of the watertable is zero) between the sea and
138 lagoon (location of the z -axis in Figure 2b,c). The segment between the sea and the internal

139 no-flow boundary is referred to as Unit 1, whereas the segment between the internal no-flow
140 and lagoon boundaries is referred to as Unit 2 (Figure 2). The widths of Units 1 and 2 are l_1
141 [L] and l_2 [L], respectively. In addition, the flow is asymmetrical in Units 1 and 2, with
142 divergent flow (the aquifer width w [L] increases along the flow direction) in Unit 1 and
143 convergent flow (w decreases along the flow direction) in Unit 2.

144 The x - z coordinate origin is placed at the intersection of the internal no-flow boundary
145 and impermeable base, with the x -axis pointing to the circle center and the z -axis pointing
146 vertically upward. Further, ϕ [L] is the watertable height, h [L] is the vertical distance
147 between the watertable and the interface, h_s [L] is the vertical distance between the sea level
148 and the interface, and $h_c = H_s - h_s$ [L] is the vertical distance from the impermeable base to
149 the interface for given x (Figure 2b,c). Constant recharge into the saturated zone, N [LT⁻¹], is
150 assumed. There are two possibilities for the interface tip (i.e., the location where the
151 freshwater-seawater interface connects to the z -axis or the bottom boundary): above the
152 aquifer bed (Figure 2b) or on the aquifer bed (Figure 2c). The x -coordinates of the interface
153 tip in Units 1 and 2 are denoted as x_{t1} [L] and x_{t2} [L], respectively (Figure 2c). Note that $x_{t1} =$
154 $x_{t2} = 0$ when the interface tip is above the aquifer bed, as in Figure 2b.

155 Consistent with previous studies (e.g., Ketabchi et al., 2014; Lu et al., 2016; 2019), the
156 following assumptions are made: (1) steady-state flow, (2) sharp freshwater-seawater
157 interface, (3) homogeneous and isotropic aquifer, (4) negligible unsaturated flow, (5) recharge
158 is less than the saturated hydraulic conductivity (else overland flow will appear following

Formatted: English (United States)

Deleted: which

160 ponding), and (6) vertical flow in the saturated zone is negligible (Dupuit-Forchheimer
 161 approximation).

162 3. Analytical Solutions

163 Groundwater flow in an ASA (Figure 2) can be described as (Paniconi et al., 2003; Troch
 164 et al., 2003),

$$165 \quad -\frac{\partial}{\partial x}(wq) + Nw = \frac{\partial S}{\partial t} \quad (1)$$

166 where q [L^2T^{-1}] is the Darcy flux per unit length along the aquifer, x [L] represents the
 167 distance from the circle center to the arc, S [L^2] is the total water storage per unit distance
 168 along the aquifer, and t [T] is time. Equation (1) is the so-called the hillslope-storage
 169 Boussinesq equation and was first proposed by Troch et al. (2003). For a given radial distance
 170 x , this equation assumes that the velocity is the same everywhere on the arc (w). Based on this
 171 assumption, the 3D flow problem can be simplified to 1D, making it possible to consider
 172 geometry effects analytically. Paniconi et al. (2003) validated equation (1) by comparing it
 173 with a 3D Richards' equation model and found that predictions of equation (1) matched well
 174 those of the 3D model for nine different geometries. Subsequently, equation (1) was used to
 175 for further analyses (Hilbert et al., 2005, 2007; Hazenberg et al., 2015, 2016; Kong et al.,
 176 2016; Luo et al., 2018). At steady state, equation (1) reduces to,

$$177 \quad -\frac{\partial}{\partial x}(wq) + Nw = 0 \quad (2)$$

178 According to Darcy's law and the Dupuit-Forchheimer approximation, the freshwater
 179 flux in the aquifer segment between the seaward boundary and interface tip can be calculated
 180 as (ϕ is independent of z),

Deleted: occurs

Deleted: ;

Formatted: English (United States)

Deleted:

Deleted: derived from

Deleted: T

Deleted: in

Formatted: Font: Italic

Deleted: along the x-axis direction (radial direction)

Formatted: Font: Italic

Deleted: a complicated

Deleted:

Deleted: a

Deleted: one

Deleted: by

Deleted: Richards equation

Deleted: has been

Deleted: extended

Deleted: consider different factors

Deleted:), and was implemented to the coupling model (Hilbert et al., 2007; Hazenberg et al., 2015; 2016

Deleted: , both showing satisfactory results

Formatted: English (United States)

Deleted: reformulated in terms of soil water storage rather than watertable elevation, as widely used previously (e.g., Stagnitti et al., 1986; Troch et al., 2003; Hilberts et al., 2005; Kong et al., 2016; Luo et al., 2018).

$$q = -\int_{h_c}^{\phi} K_s \frac{d\phi}{dz} dz = -K_s (\phi - h_c) \frac{d\phi}{dx} \quad (3)$$

where K_s [LT⁻¹] is the saturated hydraulic conductivity.

3.1. Interface Tip above the Aquifer Bed

We first consider the situation where the interface tip is above the aquifer bed (Figure 2b). In Unit 1 where $w = \theta(L_0 + l_2 - x)$, substituting equation (3) into equation (2) and then integrating gives,

$$-\frac{1}{2} \left[(L_0 + l_2 - x)^2 - (L_0 + l_2)^2 \right] N = -(L_0 + l_2 - x) K_s (\phi - h_c) \frac{d\phi}{dx} \quad (4)$$

According to the Ghijben-Herzberg equation, the vertical thickness of the freshwater zone (h) in the interface zone is given by,

$$h = \phi - h_c = (1 + \alpha)(\phi - H_s) \quad (5)$$

where $\alpha = \rho_f / (\rho_s - \rho_f)$ is the dimensionless density difference, and ρ_f [ML⁻³] and ρ_s [ML⁻³] are the freshwater and seawater densities, respectively. Substitution of equation (5) into equation (4) yields,

$$-\frac{1}{2} \left[(L_0 + l_2 - x)^2 - (L_0 + l_2)^2 \right] N = -K_s (L_0 + l_2 - x) (1 + \alpha) (\phi - H_s) \frac{d\phi}{dx} \quad (6)$$

Rearranging equation (6) produces,

$$-\frac{(L_0 + l_2 - x)N}{2} + \frac{N(L_0 + l_2)^2}{2(L_0 + l_2 - x)} = -K_s (1 + \alpha) (\phi - H_s) \frac{d\phi}{dx} \quad (7)$$

Integrating equation (7) leads to,

$$-\frac{(L_0 + l_2)^2 N}{2} \ln(L_0 + l_2 - x) - \frac{1}{2} (L_0 + l_2) Nx + \frac{1}{4} Nx^2 + C_1 = -K_s (1 + \alpha) \frac{(\phi - H_s)^2}{2} \quad (8)$$

where C_1 is the integration constant that is determined by the sea boundary condition (i.e.,

$x = -l_1$, $\phi = H_s$),

Deleted: (based on the Dupuit-Forchheimer approximation)

$$C_1 = \frac{(L_0 + l_2)^2 N}{2} \ln(L_0 + l_2 + l_1) - \frac{1}{2}(L_0 + l_2)l_1 N - \frac{1}{4}l_1^2 N \quad (9)$$

The relation between h_s and ϕ is given by,

$$h_s = \alpha(\phi - H_s) \quad (10)$$

Combining equation (8) with equation (10) and eliminating ϕ yields,

$$-\frac{(L_0 + l_2)^2 N}{2} \ln(L_0 + l_2 - x) - \frac{1}{2}(L_0 + l_2)Nx + \frac{1}{4}Nx^2 + C_1 = -K_s(1 + \alpha)\frac{h_s^2}{2\alpha^2} \quad (11)$$

Equation (11) gives the freshwater-seawater interface location in Unit 1 once l_1 and l_2 are determined.

Equation (8) applies to Unit 2 by replacing C_1 with C_2 ,

$$-\frac{(L_0 + l_2)^2 N}{2} \ln(L_0 + l_2 - x) - \frac{1}{2}(L_0 + l_2)Nx + \frac{1}{4}Nx^2 + C_2 = -K_s(1 + \alpha)\frac{(\phi - H_s)^2}{2} \quad (12)$$

where C_2 is chosen to satisfy the lagoon boundary condition ($x = l_2$, $\phi = H_s$),

$$C_2 = \frac{(L_0 + l_2)^2 N}{2} \ln(L_0) + \frac{1}{2}(L_0 + l_2)l_2 N - \frac{1}{4}l_2^2 N \quad (13)$$

Combining equations (10) and (12) and eliminating ϕ leads to,

$$-\frac{(L_0 + l_2)^2 N}{2} \ln(L_0 + l_2 - x) - \frac{1}{2}(L_0 + l_2)Nx + \frac{1}{4}Nx^2 + C_2 = -K_s(1 + \alpha)\frac{h_s^2}{2\alpha^2} \quad (14)$$

Equation (14) gives the freshwater-seawater interface location in Unit 2 once l_2 is determined. Since the sea level and lagoon water level are the same, an internal no-flow boundary exists between the sea and lagoon, i.e.,

$$x = 0, \quad (h_s)_{unit1} = (h_s)_{unit2} \quad (15)$$

where $(h_s)_{unit1}$ and $(h_s)_{unit2}$ represent h_s in Units 1 and 2, respectively.

Combining equations (11), (14) and (15) leads to expressions for l_1 and l_2 ,

Deleted: generates

$$l_1 = L + L_0 - \sqrt{\frac{2LL_0 + L^2}{2\ln(L + L_0) - 2\ln(L_0)}} \quad (16)$$

$$l_2 = \sqrt{\frac{2LL_0 + L^2}{2\ln(L + L_0) - 2\ln(L_0)}} - L_0 \quad (17)$$

As indicated by equations (16) and (17), the internal no-flow boundary between the sea and lagoon only depends on L and L_0 . For known l_1 and l_2 , equations (11) and (14) can be employed to predict the freshwater-seawater interface location in Units 1 and 2, respectively.

Once the interface location is determined, h and ϕ are given by,

$$h = \frac{1 + \alpha}{\alpha} h_s \quad (18)$$

$$\phi = \frac{h_s}{\alpha} + H_s \quad (19)$$

3.2. Interface Tip on the Aquifer Bed

When the interface tip is on the aquifer bed, the location of the internal no-flow boundary remains the same as for the interface tip above the aquifer bed. The freshwater-seawater interface for Units 1 and 2 can be determined by equations (11) and (14), respectively. Then, from equation (18), h at the aquifer segment between the sea boundary and the interface tip is determined. To calculate h for the aquifer segment between the interface tip and the internal no-flow boundary, the x -coordinate of the interface tip is found. At the interface tip of Unit 1 ($x = x_{i1}$),

$$h_s = H_s \quad (20)$$

$$\phi = \frac{1 + \alpha}{\alpha} H_s \quad (21)$$

With equations (11) and (21), x_{i1} is given by,

$$-\frac{(L_0 + l_2)^2 N}{2} \ln(L_0 + l_2 - x_{i1}) - \frac{1}{2}(L_0 + l_2)Nx_{i1} + \frac{1}{4}Nx_{i1}^2 = -C_1 - K_s(1 + \alpha)\frac{H_s^2}{2\alpha^2} \quad (22)$$

265 Let,

$$266 \quad a = \frac{1}{4}N \quad (23a)$$

$$267 \quad b = -\frac{1}{2}(L_0 + l_2)N \quad (23b)$$

$$268 \quad c = -\frac{(L_0 + l_2)^2 N}{2} \quad (23c)$$

269 and

$$270 \quad m = -C_1 - K_s(1 + \alpha)\frac{H_s^2}{2\alpha^2} \quad (23d)$$

271 then equation (22) becomes,

$$272 \quad ax_{i1}^2 + bx_{i1} + c \ln(L_0 + l_2 - x_{i1}) = m \quad (24)$$

273 which is solved by a root-finding method.

274 The freshwater discharge for the aquifer segment between the interface tip and the

275 internal no-flow boundary is calculated as,

$$276 \quad -\frac{1}{2}\left[(L_0 + l_2 - x)^2 - (L_0 + l_2)^2\right]N = -(L_0 + l_2 - x)K_s\phi\frac{d\phi}{dx} \quad (25)$$

277 Repeating the steps from equations (4) to (8) gives,

$$278 \quad -\frac{(L_0 + l_2)^2 N}{2} \ln(L_0 + l_2 - x) - \frac{1}{2}(L_0 + l_2)Nx + \frac{1}{4}Nx^2 + C_3 = -\frac{K_s}{2}\phi^2 \quad (26)$$

279 where C_3 is determined by substituting equation (21) into equation (26). Then, equation (26)

280 can be adopted to calculate h for the segment between the interface tip and the internal no-

281 flow boundary where $h = \phi$.

282 Similarly, the x -coordinate of the interface tip in Unit 2 (x_{i2}) is obtained by substituting

283 equation (20) into equation (14). Then, the watertable (h) of the aquifer segment between the

284 interface tip and the internal no-flow boundary for Unit 2 is computed by repeating the steps

285 from equations (22) to (26).

286 4. Results and Discussion

287 4.1. Validation of the Analytical Solutions

288 The analytical solutions were validated by comparing their predictions with experimental
289 data compiled from Memari et al. (2020), who reported experiments carried out using a 15°
290 radial tank. The tank contained three distinct chambers: internal no-flow boundary condition,
291 porous medium and constant-head boundary condition (i.e., sea or lagoon). The internal no-
292 flow and seaward boundaries were respectively located at 10 cm and 55.5 cm from the circle
293 center, i.e., 45.5 cm from the internal no-flow boundary to the constant-head boundary along
294 the radial direction. Note that the experimental tank only corresponds to Unit 1 of the radial
295 aquifer with $l_1 = 45.5$ cm and $l_2 = 0$, so the analytical results were calculated using
296 equations (11) and (24). The thicknesses of the porous medium and sea level were 28 and 25
297 cm, respectively, with $K_s = 1.23 \times 10^{-2}$ m s⁻¹. The measured saltwater and freshwater densities
298 were respectively 1.015 and 0.999 g ml⁻¹, leading to $\alpha = 62$. Two different recharge events
299 with constant N , 2.46×10^{-4} and 1.08×10^{-4} m s⁻¹, were considered in the experiments.

300 Figure 3 shows the comparison between analytical and experimental results of the
301 freshwater-seawater interface for different recharge events. In general, the analytical solution
302 predicts the freshwater-seawater interface well for both recharge events, despite there being
303 some differences between the analytical results and the measurements, particularly in the zone
304 near the constant-head boundary ($x = -45$ cm). These deviations are likely due to assumptions
305 made in the analytical solution, i.e., (i) a sharp freshwater-seawater interface, (ii) ignoring the

Deleted: . The sand used in experiments had

Deleted: a saturated hydraulic conductivity of

Formatted: Font: Italic, Subscript

Deleted: and an effective porosity of 0.40

Formatted: Font: Italic

309 effect of freshwater discharge, and (iii) neglecting the vertical flow (the Dupuit-Forchheimer
310 approximation).

311 **4.2. Effects of Aquifer Geometry on Seawater Intrusion**

312 Previous studies showed that boundary conditions play a critical role in estimates of
313 seawater intrusion (Werner & Simmons, 2009; Lu et al., 2016). Therefore, the internal no-
314 flow boundary between the sea and lagoon was examined for various ASAs. As indicated by
315 equations (16) and (17), this internal no-flow boundary depends only on L and L_0 . The values
316 of l_1 and l_2 calculated respectively from equations (16) and (17) are shown in Figure 4 for
317 three typical values of L (500, 1000 and 2000 m) with L_0 varying from 10^2 to 10^6 m. In
318 general, the internal no-flow boundary deviates from the middle of the ASA. When L_0 is less
319 than 10^5 m, l_1 is larger than l_2 for the three different values of L , indicating an internal no-
320 flow boundary closer to the lagoon boundary. For example, taking $L = 2000$ m and $L_0 = 100$ m
321 leads to $l_1 = 1240$ m and $l_2 = 760$ m, with a deviation of 240 m (12% of 2000 m) from the
322 middle of the ASA. When L_0 exceeds 10^5 m, however, the location of the internal no-flow
323 boundary can be approximated as being at the middle of the ASA for all considered values of
324 L . This is in contrast to strip and circular aquifers where the internal no-flow boundary is
325 always in the middle of aquifers due to symmetry.

326 Since the internal no-flow boundary location between the sea and lagoon deviates from
327 the middle of the ASA, we expect aquifer geometry to play a significant role in controlling
328 seawater intrusion. As mentioned previously, ASAs can be convergent (Unit 1) or divergent
329 aquifers (Unit 2) where the extent of seawater intrusion may be different. However, for strip

330 aquifers, both Units 1 and 2 are rectangular with the same extent of seawater intrusion.
331 Therefore, three geometries were compared in this study: convergent, rectangular and
332 divergent (Figure 5). These geometries have been widely examined in hillslope hydrology
333 regrading to the effects of aquifer geometry on runoff generation (Troch et al., 2003; Kong et
334 al., 2016; Luo et al., 2018). To present the results more conveniently, we replaced the x - z
335 coordinate origin at the intersection of the constant-head boundary (sea or lagoon) and the
336 impermeable base, with the x -axis pointing horizontally to the internal no-flow boundary and
337 the z -axis vertically upward (Figure 5). In addition, the distance between the constant-head
338 boundary and the internal no-flow boundary (aquifer width) is denoted as L^* (Figure 5) while
339 the other parameters remain the same.

340 Following previous studies (e.g., Lu et al., 2016; 2019), different cases were selected to
341 show the effects of aquifer geometry on seawater intrusion (Cases 1 and 2 in Table 1).
342 According to Werner et al. (2017), the width of atoll islands generally varies from 100 to 1500
343 m along the radial direction. In order to focus on the effects of aquifer geometry on seawater
344 intrusion, the same L^* and L_0 were assumed for the three aquifers, with L^* and L_0 equal to
345 1000 and 200 m, respectively. Note that L_0 is the distance from the circle center to the lagoon
346 boundary for convergent aquifers, whereas it represents the distance from the circle center to
347 internal no-flow boundary for divergent aquifers hereafter. The sand characteristics were the
348 same as in the experiments of Memari et al. (2020). Two recharge events were considered
349 (Cases 1 and 2, Table 1). The freshwater-seawater interface was calculated using the
350 analytical solutions for the three different aquifers. Note that the Appendix presents analytical

351 solutions for seawater intrusion in strip aquifers deduced from Lu et al. (2019).

352 Figure 6 shows the freshwater-seawater interface calculated for Cases 1 and 2. As can be
353 seen, the extent of seawater intrusion is noticeably different for the three aquifer geometries.
354 For high recharge ($1 \times 10^{-6} \text{ m s}^{-1}$), the interface tip is located at around 500 m for the
355 divergent aquifer, which is about twice the value of the rectangular aquifer and six times the
356 value for the convergent aquifer (Figure 6a). When the recharge decreases to $3 \times 10^{-7} \text{ m s}^{-1}$,
357 the interface tip moves further landward for the three aquifers as expected, but the difference
358 between results is still great (Figure 6b). The interface tip is displaced above the aquifer bed
359 for both the rectangular and divergent aquifers, while it remains on the aquifer bed for the
360 convergent aquifer. Regardless of the recharge rate, the most landward freshwater-seawater
361 interface occurs in the divergent aquifer and vice versa for the convergent aquifer. This
362 underlines that aquifer geometry plays a major role in controlling seawater intrusion and
363 hence it is necessary to account for aquifer geometry in analyses of seawater intrusion.

364 4.3. Sensitivity Analysis

365 A sensitivity analysis was conducted to investigate to what extent aquifer geometry
366 affects seawater intrusion. Since we focus on the effects of aquifer geometry on the locations
367 of the freshwater-seawater interface and watertable, values of L_0 and L^* were varied, with
368 other parameters kept constant. When conducting the sensitivity analysis of L_0 , L^* was fixed
369 at 1000 m, which is a typical value for ASAs (Werner et al., 2017). Figure 7 shows the
370 sensitivity of the locations of the freshwater-seawater interface and watertable to changes in
371 L_0 (Case 3, Table 1). The freshwater-seawater interface and watertable elevation are

372 independent of L_0 for rectangular aquifers (Appendix). However, the freshwater-seawater
373 interface and watertable elevation differ greatly when varying L_0 for both convergent and
374 divergent aquifers, highlighting that L_0 plays an important role in affecting seawater intrusion.
375 Specifically, as L_0 increases, the freshwater-seawater interface moves more landward (larger
376 x/L^* , Figure 7a) and its corresponding watertable elevation decreases (Figure 7c) for
377 convergent aquifers. In contrast, for divergent aquifers increasing L_0 moves the freshwater-
378 seawater interface more seaward (smaller x/L^* , Figure 7b) and its corresponding watertable
379 elevation increases (Figure 7d). For a given L_0 , divergent aquifers have the largest extent of
380 seawater intrusion and the lowest watertable elevation, and conversely for convergent aquifers
381 (Figure 7).

382 Regardless of the freshwater-seawater interface and watertable elevation, the deviation
383 between rectangular aquifers and divergent or convergent aquifers is significant when L_0 is
384 less than 2000 m (Figure 7). For example, the x -coordinate of the interface tip ($z = 0$) is 262 m
385 for the rectangular aquifer at $L_0 = 200$ m, whereas it is 78 (31% of that in the rectangular
386 aquifer) and 500 m (191% of that in the rectangular aquifer) for the convergent and divergent
387 aquifers, respectively. As L_0 increases, the deviation between the three aquifers decreases.
388 When $L_0 = 2000$ m, the x -coordinate of the interface tip is 262, 209 (80% of that in the
389 rectangular aquifer) and 318 m (121% of that in the rectangular aquifer) for the rectangular,
390 convergent and divergent aquifers, respectively. As L_0 increases to 6000 m, the freshwater-
391 seawater interface and watertable elevation of both convergent and divergent aquifers tend to
392 those of rectangular aquifers, i.e., geometry effects decrease with increasing L_0 . These results

393 highlight the critical role played by the shape of aquifers. As a result, ignoring the aquifer
394 geometry may lead to an inappropriate management strategy for groundwater resources in
395 atoll islands.

Deleted: effects

396 The sensitivity of the freshwater-seawater interface and watertable elevation to L^* was
397 investigated by varying L^* from 600 to 1600 m while fixing L_0 to 200 m (Case 4, Table 1). As
398 shown in Figure 8, contrary to the results for varying L_0 , in this case the freshwater-seawater
399 interface and watertable elevation in all three topographies are related to L^* . Again, the extent
400 of seawater intrusion is greatest in divergent aquifers and least in convergent aquifers for
401 given L^* . When L^* increases, the freshwater-seawater interface moves seaward and the
402 watertable elevation increases, regardless of aquifer geometry, i.e., the seawater intrusion
403 decreases (Figures 8a-c). This is because the total freshwater flux increases with increasing
404 L^* , leading to a higher hydraulic gradient and hence less seawater intrusion (Figures 8d-f).

405 Moreover, an increase in L^* reduces the differences in the seawater intrusion distance among
406 the three geometries, i.e., the effects of aquifer geometry on seawater intrusion are more
407 significant at small L^* . However, even at the maximum L^* considered (1600 m), the deviation
408 between three aquifers remains significant: The x -coordinate of the interface tip is about 148
409 m for the rectangular aquifer, whereas it is about 32 (22% of that in the rectangular aquifer)
410 and 278 m (188% of that in the rectangular aquifer) for the convergent and divergent aquifers,
411 respectively. Both L_0 and L^* can greatly impact seawater intrusion estimates for divergent and
412 convergent aquifers, highlighting the necessity to include geometry effects in analytical
413 solutions of seawater intrusion.

Deleted: effects

5. Conclusions

Based on the Ghijben-Herzberg and hillslope-storage Boussinesq equations, we derived analytical solutions of steady-state seawater intrusion for ASAs, with a focus on the freshwater-seawater interface and its corresponding watertable elevation as affected by recharge. After comparing with experimental data of Memari et al. (2020), the analytical solutions were employed to examine the effects of aquifer geometry on seawater intrusion in island aquifers. Three different shapes of island aquifer were compared: convergent, rectangular and divergent. The results lead to the following conclusions:

- The presented analytical solutions perform well in predicting the experimental freshwater-seawater interface, suggesting that these analytical solutions can predict seawater intrusion reasonably in different aquifer geometries.
- Island geometry plays a significant role in affecting the freshwater-seawater interface and watertable elevation. Other factors being equal, the extent of seawater intrusion is greatest in divergent aquifers, and conversely least in convergent aquifers. In contrast, the watertable elevation is lowest in divergent aquifers and highest in convergent aquifers.
- The effects of aquifer geometry on seawater intrusion are dependent on the aquifer width and distance from the circle center to the internal no-flow boundary (Figures 7 and 8). A larger aquifer width and distance from the circle center to the inner arc (the lagoon boundary for convergent aquifers while the internal no-flow boundary for divergent aquifers) weakens the role played by aquifer geometry and hence lead to a smaller deviation of the extent of seawater intrusion between the three topographies.

Deleted: (1)

Formatted: Font: 12 pt

Formatted: List Paragraph, Indent: Left: 0 cm, Hanging: 0.5 cm, Bulleted + Level: 1 + Aligned at: 1.48 cm + Indent at: 2.12 cm

Deleted: (2)

Deleted: (3)

440 Real island aquifers are expected to exhibit more complexity than considered here, e.g.,
441 that will have more complex shapes and are subjected to transient flow conditions caused by
442 tides, waves and groundwater pumping (Mantoglou et al. 2003; Pool & Carrera., 2011;
443 Werner et al., 2013). In addition, since the experimental scale of Memari et al. (2020) is
444 necessarily small, future experiments and field data are needed to further validate and
445 facilitate the analytical solutions. Despite this, the new analytical solutions, validated against
446 experiments, can be used as a tool for rapid estimation of seawater intrusion in ASAs once
447 known island geometry and corresponding soil properties are given.

Deleted: to rapidly estimate

449 **Appendix: Analytical Solutions for Rectangular Aquifers**

450 For rectangular aquifers, the seawater intrusion in Unit 1 is identical to that in Unit 2
 451 because of symmetry. With the interface tip on the aquifer bed, analytical solutions for the
 452 freshwater-seawater interface (h_s), watertable elevation (h), and x -coordinate of the interface
 453 tip in Unit 2 (x_{i2}) can be respectively written as (Lu et al., 2019),

$$454 \quad h_s = \alpha \sqrt{\frac{N}{(1+\alpha)K_s} \left(\frac{L^2}{4} - x^2 \right)} \quad (\text{A1})$$

$$455 \quad h = \begin{cases} \sqrt{\frac{N}{K_s} (x_{i2}^2 - x^2) + \left(\frac{H_s}{\alpha} + H_s \right)} & 0 \leq x \leq x_{i2} \\ \sqrt{\frac{N}{(1+\alpha)K_s} \left(\frac{L^2}{4} - x^2 \right) + H_s} & x_{i2} < x \leq \frac{L}{2} \end{cases} \quad (\text{A2})$$

$$456 \quad x_{i2} = \sqrt{\frac{L^2}{4} - \frac{(1+\alpha)K_s}{N} \left(\frac{H_s^2}{\alpha^2} \right)} \quad (\text{A3})$$

457 When the interface tip is above the aquifer bed, the analytical solution for the freshwater-
 458 seawater interface location and watertable elevation in Unit 2 are the same as equations (A1)
 459 and (A2), respectively.

460 **Code/Data availability**

461 Experimental data used in this study are compiled from Memari et al. (2020).

462 **Author contributions**

463 All authors contributed to the design of the research. ZL carried out data collation,
464 developed the analytical solutions and prepared the manuscript with contributions from all
465 co-authors. All authors contributed to the interpretation of the results and provided feedback.

466 **Competing interests**

467 The authors declare that they have no conflicts of interest.

468 **Acknowledgments**

469 This research was supported by the National Key R&D Program of China
470 (2019YFC0409004) and the National Natural Science Foundation of China (51979095 and
471 41807178). ZL acknowledges EPFL for financial support and JK acknowledges the Qing Lan
472 Project of Jiangsu Province (2020).

473 **References**

474 Ayers, J. F., & Vacher, H. L. (1986). Hydrogeology of an atoll island: A conceptual model
475 from detailed study of a Micronesian example. *Groundwater*, 24(2), 185-198.

476 <https://doi.org/10.1111/j.1745-6584.1986.tb00994.x>

Formatted: Font: 12 pt

477 Bailey, R. T., Jenson, J. W., & Olsen, A. E. (2010). Estimating the ground water resources of
478 atoll islands. *Water*, 2(1), 1-27. <https://doi.org/10.3390/w2010001>

Formatted: Font: 12 pt

479 Bailey, R. T., Jenson, J. W., & Olsen, A. E. (2009). Numerical modeling of atoll island
480 hydrogeology. *Groundwater*, 47(2), 184-196. <https://doi.org/10.1111/j.1745->

Formatted: Font: 12 pt

481 [6584.2008.00520.x](https://doi.org/10.1111/j.1745-6584.2008.00520.x)

482 Bedekar, V. S., Memari, S. S., & Clement, T. P. (2019). Investigation of transient freshwater
483 storage in island aquifers. *Journal of Contaminant Hydrology*, 221, 98-107.

484 <https://doi.org/10.1016/j.jconhyd.2019.02.004>

Formatted: Font: 12 pt

485 Chesnaux, R., & Allen, D. M. (2008). Groundwater travel times for unconfined island
486 aquifers bounded by freshwater or seawater. *Hydrogeology Journal*, 16(3), 437-445.

487 <https://doi.org/10.1007/s10040-007-0241-6>

Formatted: Font: 12 pt

488 Dose, E. J., Stoeckl, L., Houben, G. J., Vacher, H. L., Vassolo, S., Dietrich, J., &
489 Himmelsbach, T. (2014). Experiments and modeling of freshwater lenses in layered
490 aquifers: Steady state interface geometry. *Journal of Hydrology*, 509, 621-630.

491 <https://doi.org/10.1016/j.jhydrol.2013.10.010>

Formatted: Font: 12 pt

492 Drabbe J. & Badon Ghijben, W. (1889). *Nota in verband met de voorgenomen put boring*
493 *nabij Amsterdam*. Tijdschrift van het Koninklijk Instituut van Ingenieurs. pp. 8-22,

Formatted: Dutch (Netherlands)

Gravenhage, Netherlands.

Duvat, V. K. E. (2019). A global assessment of atoll island planform changes over the past decades. *Wiley Interdisciplinary Reviews: Climate Change*, 10(1), e557.

<https://doi.org/10.1002/wcc.557>

Formatted: Font: 12 pt

Fetter, C. W. (1972). Position of the saline water interface beneath oceanic islands. *Water Resources Research*, 8(5), 1307-1315. <https://doi.org/10.1029/WR008i005p01307>

Formatted: Font: 12 pt

Gingerich, S. B., Voss, C. I., & Johnson, A. G. (2017). Seawater-flooding events and impact on freshwater lenses of low-lying islands: Controlling factors, basic management and mitigation. *Journal of Hydrology*, 551, 676-688.

<https://doi.org/10.1016/j.jhydrol.2017.03.001>

Formatted: Font: 12 pt

Greskowiak, J., Röper, T., & Post, V. E. (2013). Closed-form approximations for two-dimensional groundwater age patterns in a fresh water lens. *Groundwater*, 51(4), 629-634. <https://doi.org/10.1111/j.1745-6584.2012.00996.x>

Formatted: No underline, Font color: Auto

Formatted: Font: 12 pt

Hazenberg, P., Fang, Y., Broxton, P., Gochis, D., Niu, G. Y., Pelletier, J. D., Troch., P. A., & Zeng, X. (2015). A hybrid-3D hillslope hydrological model for use in Earth system models. *Water Resources Research*, 51(10), 8218-8239.

Formatted: Font: Italic

Formatted: Font: Italic

<https://doi.org/10.1002/2014WR016842>

Deleted: *** hyperlink ***

Hazenberg, P., Broxton, P., Gochis, D., Niu, G. Y., Pangle, L. A., Pelletier, J. D., Troch., P. A., & Zeng, X. (2016). Testing the hybrid-3-D hillslope hydrological model in a controlled environment. *Water Resources Research*, 52(2), 1089-1107.

Formatted: Font: 12 pt

Formatted: Font: Italic

Formatted: Font: Italic

<https://doi.org/10.1002/2015WR018106>

Deleted: *** hyperlink ***

517 Herzberg, A. (1901). Die wasserversorgung einiger Nordseebäder. *Journal für*
518 *Gasbeleuchtung und Wasserversorgung*, 44, 815-819, 45, 842-844.

519 Hilberts, A. G. J., Troch, P. A., & Paniconi, C. (2005). Storage-dependent drainable porosity
520 for complex hillslopes. *Water Resources Research*, 41(6), W06001.
521 <https://doi.org/10.1029/2004WR003725>

522 Hilberts, A. G., Troch, P. A., Paniconi, C., & Boll, J. (2007). Low-dimensional modeling of
523 hillslope subsurface flow: Relationship between rainfall, recharge, and unsaturated
524 storage dynamics. *Water Resources Research*, 43(3), W03445.
525 <https://doi.org/10.1029/2006WR004964>

526 Ketabchi, H., Mahmoodzadeh, D., Ataie-Ashtiani, B., Werner, A. D., & Simmons, C. T.
527 (2014). Sea-level rise impact on fresh groundwater lenses in two-layer small islands.
528 *Hydrological Processes*, 28(24), 5938-5953. <https://doi.org/10.1002/hyp.10059>

529 Kong, J., Shen, C., Luo, Z., Hua, G., & Zhao, H. (2016). Improvement of the hillslope-storage
530 Boussinesq model by considering lateral flow in the unsaturated zone. *Water*
531 *Resources Research*, 52(4), 2965-2984. <https://doi.org/10.1002/2015WR018054>

532 Lam, R. K. (1974). Atoll permeability calculated from tidal diffusion. *Journal of Geophysical*
533 *Research*, 79(21), 3073-3081. <https://doi.org/10.1029/JC079i021p03073>

534 Liu, J., & Tokunaga, T. (2019). Future risks of tsunami-induced seawater intrusion into
535 unconfined coastal aquifers: Insights from numerical simulations at Niijima Island,
536 Japan. *Water Resources Research*, 55(12), 10082-10104.
537 <https://doi.org/10.1029/2019WR025386>

- Formatted: Dutch (Netherlands)
- Formatted: No underline, Font color: Auto
- Formatted: Font: 12 pt
- Formatted: Font color: Text 1, English (United States)
- Formatted: Normal, Indent: Left: 0 cm, Hanging: 2.95 ch, First line: -2.95 ch
- Formatted: Font: Italic, Font color: Text 1, English (United States)
- Formatted: Font color: Text 1
- Formatted: Font: Italic, Font color: Text 1, English (United States)
- Formatted: Font color: Text 1
- Formatted: Font: Italic, Font color: Text 1, English (United States)
- Formatted: Font color: Text 1, English (United States)
- Formatted: Font: Italic, Font color: Text 1, English (United States)
- Formatted: Font color: Text 1, English (United States)
- Formatted: Font: 12 pt, Font color: Text 1
- Formatted: Font color: Text 1, English (United States)
- Formatted: Font: 12 pt, Font color: Text 1
- Formatted: Font: 12 pt
- Deleted: *** fix journal title ***
- Formatted: Font: (Asian) DengXian, Font color: Blue
- Formatted: Font: 12 pt
- Formatted: Font: 12 pt
- Formatted: Font: 12 pt
- Formatted: Font: 12 pt

539 Liu, Y., X. Mao, J. Chen, and D. A. Barry. 2014. Influence of a coarse interlayer on seawater
540 intrusion and contaminant migration in coastal aquifers. *Hydrological Processes*, 28(20),
541 5162-5175. <https://dx.doi.org/10.1002/hyp.10002>

Formatted: Font: 12 pt

542 Lu, C., Cao, H., Ma, J., Shi, W., Rathore, S. S., Wu, J., & Luo, J. (2019). A proof-of-concept
543 study of using a less permeable slice along the shoreline to increase fresh groundwater
544 storage of oceanic islands: Analytical and experimental validation. *Water Resources
545 Research*, 55(8), 6450-6463. <https://doi.org/10.1029/2018WR024529>

Formatted: Font: 12 pt

546 Lu, C., Xin, P., Kong, J., Li, L., & Luo, J. (2016). Analytical solutions of seawater intrusion in
547 sloping confined and unconfined coastal aquifers. *Water Resources Research*, 52(9),
548 6989-7004. <https://doi.org/10.1002/2016WR019101>

Formatted: Font: 12 pt

549 Luo, Z., Shen, C., Kong, J., Hua, G., Gao, X., Zhao, Z., Zhao, H., & Li, L. (2018). Effects of
550 unsaturated flow on hillslope recession characteristics. *Water Resources Research*,
551 54(3), 2037-2056. <https://doi.org/10.1002/2017WR022257>

Formatted: Font: 12 pt

552 Mantoglou, A. (2003). Pumping management of coastal aquifers using analytical models of
553 saltwater intrusion. *Water Resources Research*, 39(12), 1335.
554 <https://doi.org/10.1029/2002WR001891>

Formatted: Font: 12 pt

555 Memari, S. S., Bedekar, V. S., & Clement, T. P. (2020). Laboratory and numerical
556 investigation of saltwater intrusion processes in a circular island aquifer. *Water
557 Resources Research*, 56(2), e2019WR025325. <https://doi.org/10.1029/2019WR025325>

Formatted: Font: 12 pt

558 Morgan, L. K., & Werner, A. D. (2014). Seawater intrusion vulnerability indicators for
559 freshwater lenses in strip islands. *Journal of Hydrology*, 508, 322-327.

560

<https://doi.org/10.1016/j.jhydrol.2013.11.002>

Formatted: Font: 12 pt

561

Paniconi, C., Troch, P. A., Van Loon, E. E., & Hilberts, A. G. (2003). Hillslope-storage

562

Boussinesq model for subsurface flow and variable source areas along complex

563

hillslopes: 2. Intercomparison with a three-dimensional Richards equation model.

564

Water Resources Research, 39(11), 1317. <https://doi.org/10.1029/2002WR001730>

Formatted: Font: 12 pt

565

Pool, M., & Carrera, J. (2011). A correction factor to account for mixing in Ghyben-Herzberg

566

and critical pumping rate approximations of seawater intrusion in coastal aquifers.

567

Water Resources Research, 47(5), W05506. <https://doi.org/10.1029/2010WR010256>

Formatted: Font: 12 pt

568

Post, V. E. (2018). Annotated translation of “Nota in verband met de voorgenomen putboring

Formatted: Dutch (Netherlands)

569

nabij Amsterdam [Note concerning the intended well drilling near Amsterdam]” by J.

570

Drabbe and W. Badon Ghijben (1889). *Hydrogeology Journal*, 26(6), 1771-1788.

571

<https://doi.org/10.1007/s10040-018-1797-z>

Formatted: Font: 12 pt

572

Post, V. E. A., Houben, G. J., Stoeckl, L., & Sültenfuß, J. (2019). Behaviour of tritium and

Formatted: English (United States)

573

tritogenic helium in freshwater lens groundwater systems: Insights from Langeoog

574

Island, Germany. *Geofluids*, Volume 2019, Article ID 1494326. <https://doi.org/10.1155/2019/1494326>

575

<https://doi.org/10.1155/2019/1494326>

Deleted: *** Fix citation style (match the other refs) ***
<https://doi.org/10.1155/2019/1494326>

576

Röper, T., Greskowiak, J., Freund, H., & Massmann, G. (2013). Freshwater lens formation

Formatted: Default Paragraph Font, Font: 7 pt

577

below juvenile dunes on a barrier island (Spiekeroog, Northwest Germany). *Estuarine,*

578

Coastal and Shelf Science, 121-122, 40-50. <https://doi.org/10.1016/j.ecss.2013.02.004>

Formatted: Font: 12 pt

579

Stoeckl, L., Houben, G. J., & Dose, E. J. (2015). Experiments and modeling of flow processes

Deleted: Stagnitti, F., Parlange, M. B., Steenhuis, T. S., & Parlange, J.-Y. (1986). Drainage from a uniform soil layer on a hillslope. *Water Resources Research*, 22(5), 631-634. <https://doi.org/10.1029/WR022i005p00631>

580

in freshwater lenses in layered island aquifers: Analysis of age stratification, travel

Formatted: Font: 12 pt

587 times and interface propagation. *Journal of Hydrology*, 529, 159-168.

588 <https://doi.org/10.1016/j.jhydrol.2015.07.019>

Formatted: Font: 12 pt

589 Storlazzi, C. D., Gingerich, S. B., van Dongeren, A., Cheriton, O. M., Swarzenski, P. W.,
590 Quataert, E., Voss, C. I., Field, D. W., Annamalai, H., Piniak, G. A., & McCall, R.
591 (2018). Most atolls will be uninhabitable by the mid-21st century because of sea-level
592 rise exacerbating wave-driven flooding. *Science Advances*, 4(4), eaap9741.

593 <https://doi.org/10.1126/sciadv.aap9741>

Formatted: Font: 12 pt

594 Strack, O. D. L. (1976). A single-potential solution for regional interface problems in coastal
595 aquifers. *Water Resources Research*, 12(6), 1165-1174.

596 <https://doi.org/10.1029/WR012i006p01165>

Formatted: Font: 12 pt

597 Stuyfzand, P. J. (2017). Observations and analytical modeling of freshwater and rainwater
598 lenses in coastal dune systems. *Journal of Coastal Conservation*, 21(5), 577-593.

599 <https://doi.org/10.1007/s11852-016-0456-6>

Formatted: Font: 12 pt

600 Stuyfzand, P. J. (1993). *Hydrochemistry and hydrology of the coastal dune area of the Western*
601 *Netherlands*. Ph.D. Thesis. Vrije University, Amsterdam, KIWA, ISBN 90-74741-01-
602 0. <http://dare.ubvu.vu.nl/handle/1871/12716>.

Formatted: Font: 12 pt

603 Thomas, A., Baptiste, A., Martyr-Koller, R., Pringle, P., & Rhiney, K. (2020). Climate change
604 and small island developing states. *Annual Review of Environment and Resources*,
605 45(1), 1-27. <https://doi.org/10.1146/annurev-environ-012320-083355>

Formatted: Font: 12 pt

606 Troch, P. A., Paniconi, C., & Emiel van Loon, E. (2003). Hillslope-storage Boussinesq model
607 for subsurface flow and variable source areas along complex hillslopes: 1.

Deleted: *** Is it the journal style to have lower case in
PhD thesis titles? ***

610 Formulation and characteristic response. *Water Resources Research*, 39(11), 1316.

611 <https://doi.org/10.1029/2002WR001728>

Formatted: Font: 12 pt

612 Underwood, M. R., Peterson, F. L., & Voss, C. I. (1992). Groundwater lens dynamics of atoll
613 islands. *Water Resources Research*, 28(11), 2889-2902.

614 <https://doi.org/10.1029/92WR01723>

Formatted: Font: 12 pt

615 Vacher, H. L. 1988. Dupuit-Ghyben-Herzberg analysis of strip-island lenses. *Geological*

616 *Society of America Bulletin*, 100, 580-591. <https://doi.org/10.1130/0016->

617 [7606\(1988\)100<0580:DGHAOS>2.3.CO;2](https://doi.org/10.1130/0016-7606(1988)100<0580:DGHAOS>2.3.CO;2)

Formatted: Font: 12 pt

Formatted: Font: 12 pt

618 Werner, A. D., Sharp, H. K., Galvis, S. C., Post, V. E., & Sinclair, P. (2017). Hydrogeology
619 and management of freshwater lenses on atoll islands: Review of current knowledge
620 and research needs. *Journal of Hydrology*, 551, 819-844.

621 <https://doi.org/10.1016/j.jhydrol.2017.02.047>

Formatted: Font: 12 pt

622 Werner, A. D., Bakker, M., Post, V. E., Vandenbohede, A., Lu, C., Ataie-Ashtiani, B.,

623 Simmons, C. T., & Barry, D. A. (2013). Seawater intrusion processes, investigation
624 and management: Recent advances and future challenges. *Advances in Water*

625 *Resources*, 51, 3-26. <https://doi.org/10.1016/j.advwatres.2012.03.004>

Formatted: Font: 12 pt

626 Werner, A. D., & Simmons, C. T. (2009). Impact of sea-level rise on sea water intrusion in
627 coastal aquifers. *Groundwater*, 47(2), 197-204. <https://doi.org/10.1111/j.1745->

628 [6584.2008.00535.x](https://doi.org/10.1111/j.1745-6584.2008.00535.x)

Formatted: Font: 12 pt

629 White, I., & Falkland, T. (2010). Management of freshwater lenses on small Pacific islands.

630 *Hydrogeology Journal*, 18(1), 227-246. <https://doi.org/10.1007/s10040-009-0525-0>

Formatted: Font: 12 pt

631 Zhang, Y., Li, L., Erler, D. V., Santos, I., & Lockington, D. (2016). Effects of alongshore
632 morphology on groundwater flow and solute transport in a nearshore aquifer. *Water*
633 *Resources Research*, 52(2), 990-1008. <https://doi.org/10.1002/2015WR017420>

Formatted: Font: 12 pt

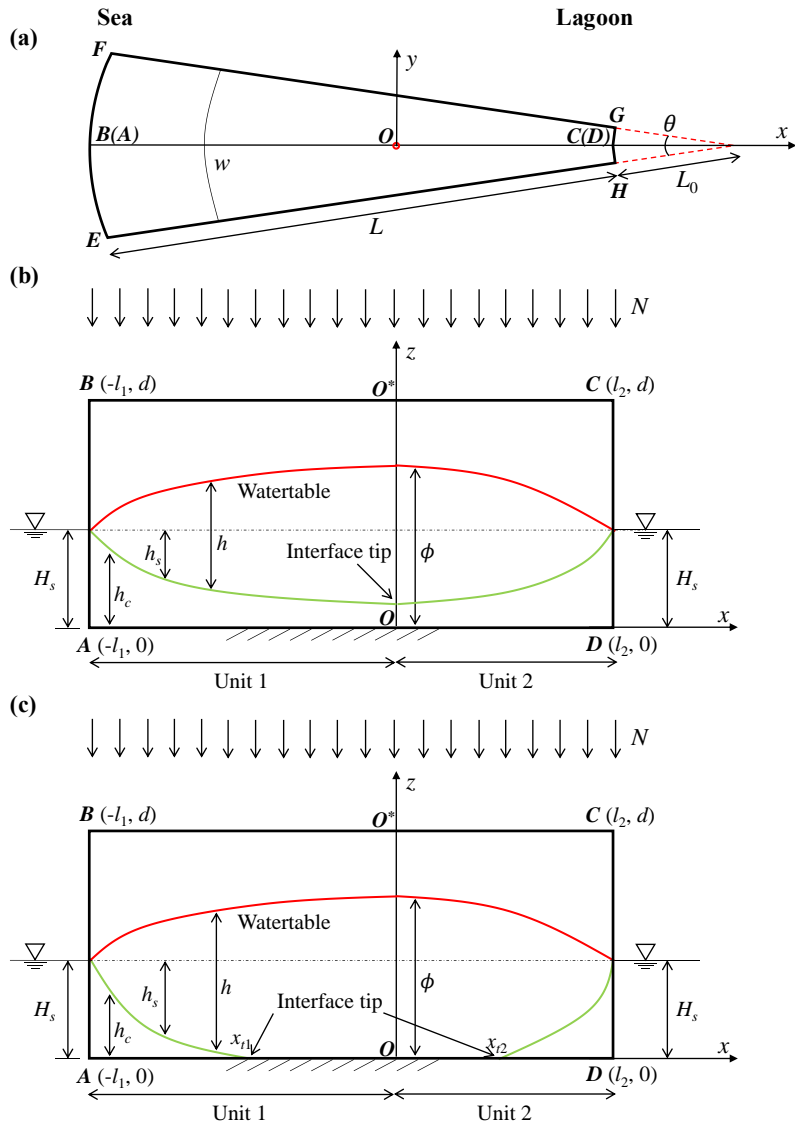
634 **Table 1.** List of parameters use in different simulations.

	No.	L^* (m)	L_0 (m)	H_s (m)	d (m)	α (-)	K_s (m s ⁻¹)	N (m s ⁻¹)
Cases	1	1000	200	38	45	40	1.23×10^{-2}	1×10^{-6}
	2	1000	200	38	45	40	1.23×10^{-2}	3×10^{-7}
	3	1000	†	38	45	40	1.23×10^{-2}	1×10^{-6}
	4	†	200	38	45	40	1.23×10^{-2}	1×10^{-6}

635 †The parameter is varied: The range of L_0 is from 200 to 6000 m, whereas the range of L^* is
636 from 600 to 1600 m.

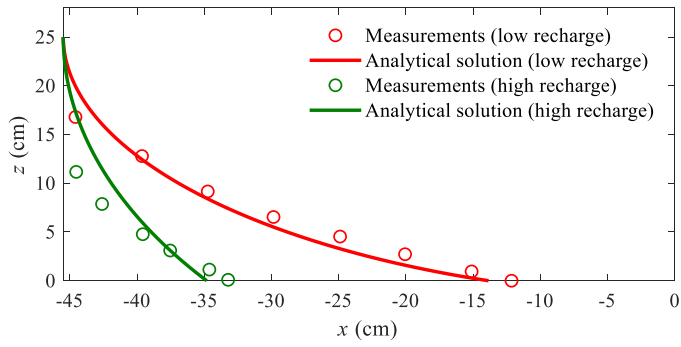


637
638 **Figure 1.** Island with an annulus segment in the Namu Atoll, Marshall Islands (© Google
639 Earth).



640
 641 **Figure 2.** Conceptual model of an annulus segment aquifer (a slice of an atoll island). (a) Plan
 642 view and (b, c) side view with the saltwater interface tip (b) above the aquifer bed (single
 643 location) and (c) on the aquifer bed (two locations). In (a), the sea boundary is on EF and the
 644 atoll lagoon boundary is on HG ; In (b) and (c), AD is the impermeable base and OO^* is the

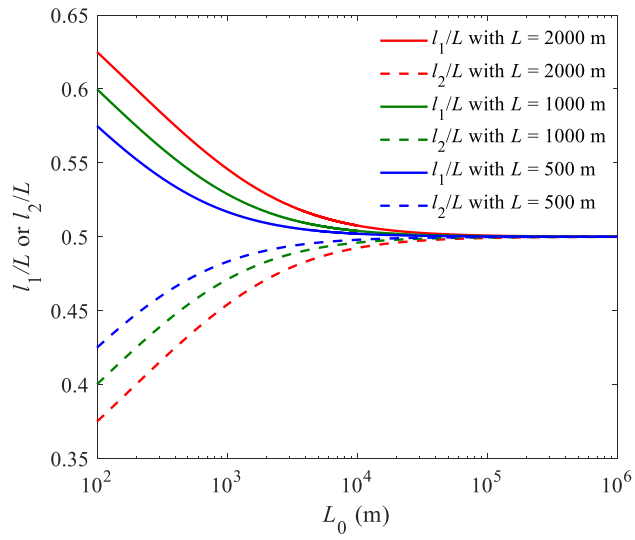
645 internal no-flow boundary.



646

647 **Figure 3.** Comparison between analytical and experimental (data compiled from Memari et
 648 al., 2020) results for the freshwater-seawater interface location for different recharge events.

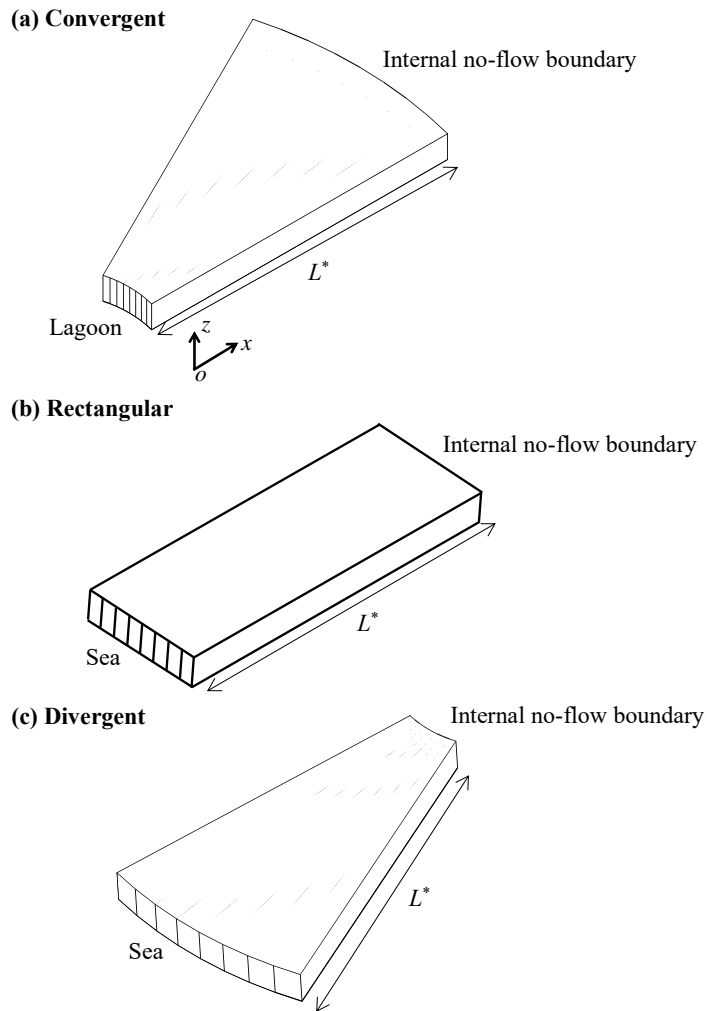
649 Note that the left and right sides are the sea and internal no-flow boundaries, respectively.



650

651

Figure 4. Widths of Unit 1 and Unit 2 versus L_0 for aquifers with different total width L .

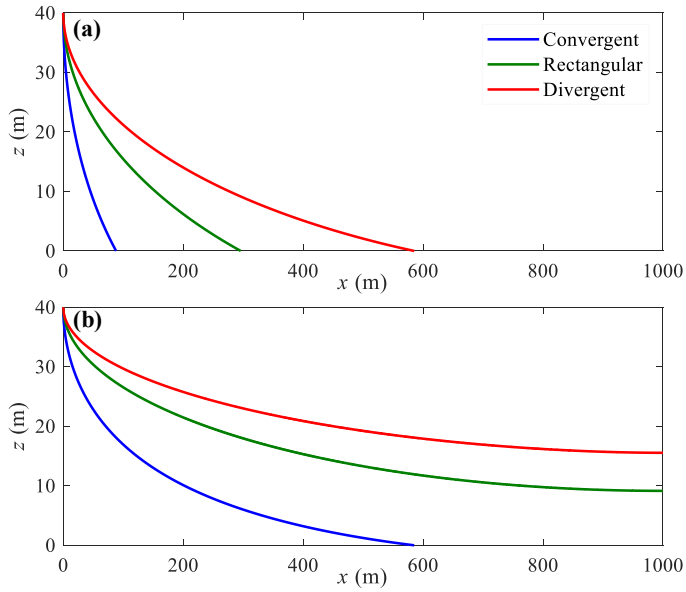


652

653

654

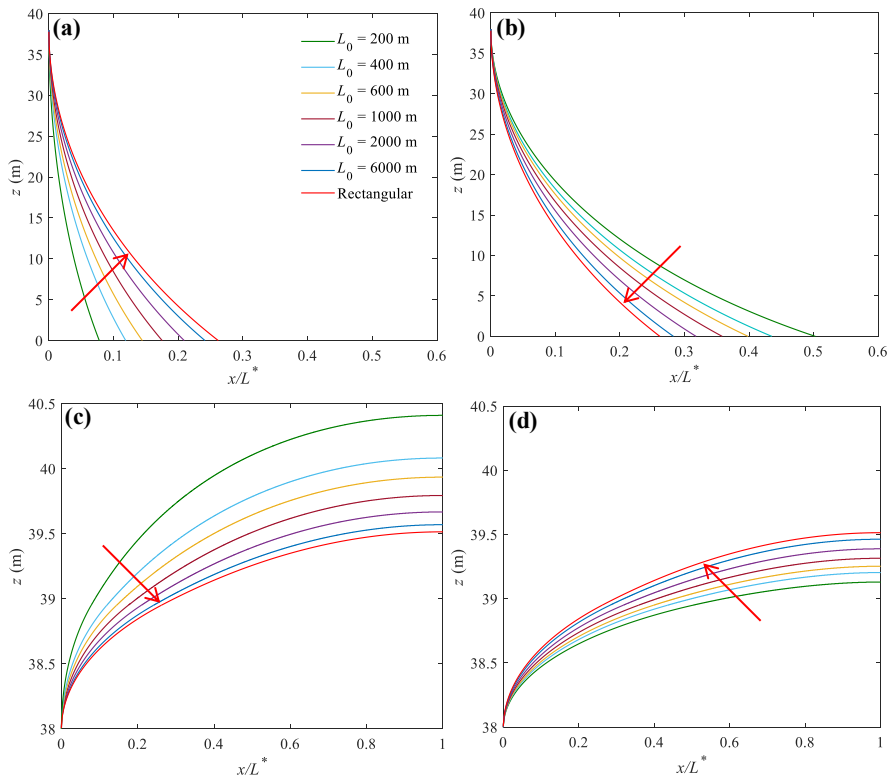
655 **Figure 5.** Three-dimensional view of (a) convergent (smaller side facing the lagoon), (b)
 656 rectangular and (c) divergent aquifers (larger side facing the sea) compared in this study. L^*
 657 represents the distance from the sea/lagoon to the internal no-flow boundary, i.e., l_1 or l_2 in
 658 Figure 2. The internal no-flow boundary corresponds to the z -axis in Figure 2.



659

660

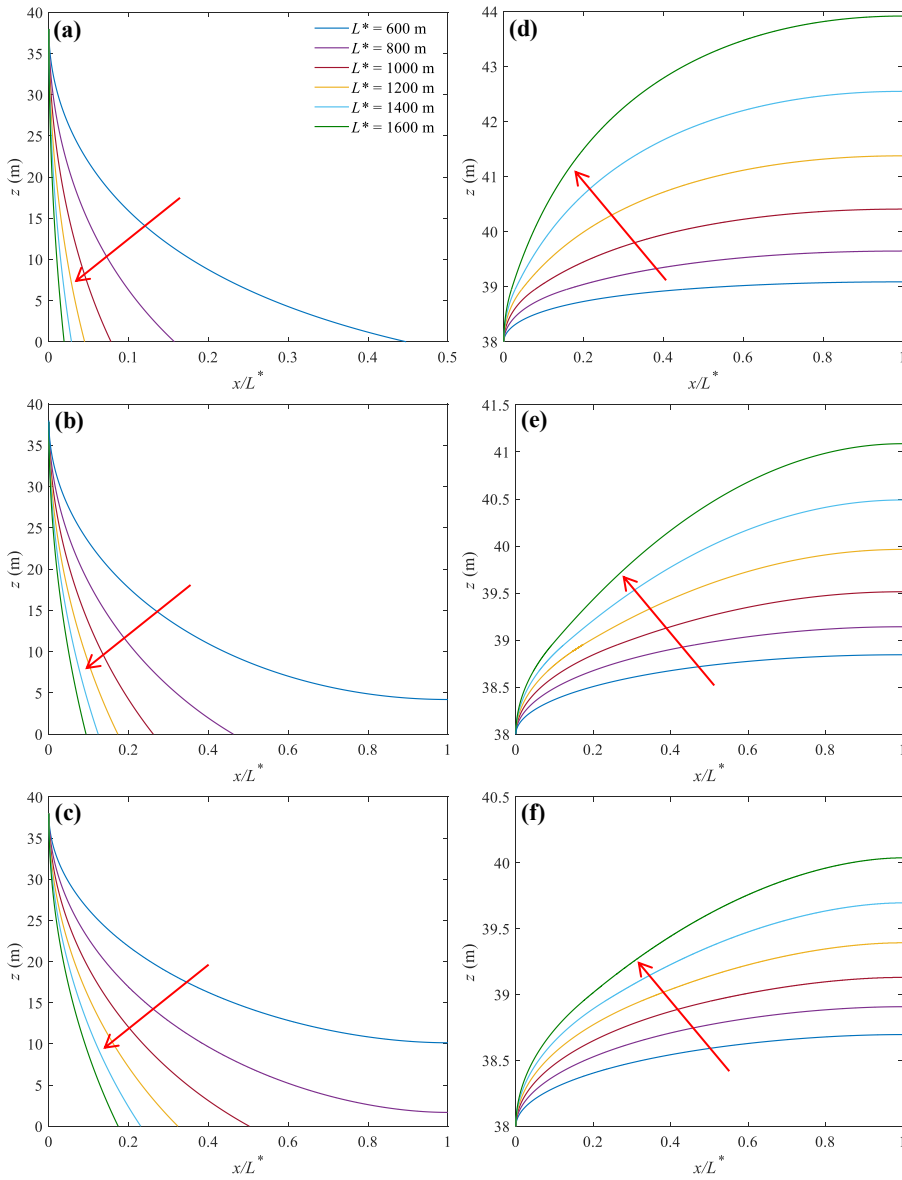
661 **Figure 6.** Freshwater-seawater interface predicted by analytical solutions for three different
 662 aquifers with (a) high and (b) low recharge (Cases 1 and 2 in Table 1). Note that $x = 1000$ m is
 663 the internal no-flow boundary in Figure 5.



664

665

666 **Figure 7.** Sensitivity of (a, b) the locations of the freshwater-seawater interface and (c, d)
 667 watertable to L_0 for convergent (left panel) and divergent (right panel) aquifers. The arrow in
 668 each plot shows the direction of increasing L_0 (values given in (a), used to produce the
 669 different curves). Note that predictions for rectangular aquifers are independent of L_0 .



673 **Figure 8.** Sensitivity of (a-c) the locations of the freshwater-seawater interface and (d-f)

674 watertable to L^* for convergent (a, d), rectangular (b, e) and divergent (c, f) aquifers. The

675 arrow in each plot points to the increase of L^* values used to construct each curve (values

676 indicated in (a)).